JACS
JOURNAL OF THE AMERICAN CHEMICAL SOCIETY
Article
pubs.acs.org/JACS

Anisotropic Growth-Induced Synthesis of Dual-Compartment Janus Mesoporous Silica Nanoparticles for Bimodal Triggered Drugs Delivery

Xiaomin Li,[†] Lei Zhou,[†] Yong Wei,[†] Ahmed Mohamed El-Toni,[‡,§] Fan Zhang,*[,†] and Dongyuan Zhao*[,†]

[†]Department of Chemistry and Laboratory of Advanced Materials, Fudan University, Shanghai 200433, P. R. China
[‡]King Abdullah Institute for Nanotechnology, King Saud University, Riyadh 11451, Saudi Arabia
[§]Central Metallurgical Research and Development Institute, CMRDI, Helwan 11421, Cairo, Egypt

Supporting Information

ABSTRACT: Multifunctional dual-compartment Janus mesoporous silica nanocomposites of UCNP@SiO_2@mSiO_2&PMO (UCNP = upconversion nanoparticle, PMO = periodic mesoporous organosilica) containing core@shell@shell structured UCNP@SiO_2@mSiO_2 nanospheres and PMO single-crystal nanocubes have been successfully synthesized via a novel anisotropic island nucleation and growth approach with the ordered mesostructure. The asymmetric Janus nanocomposites show a very uniform size of ∼300 nm and high surface area of ∼1290 m^2/g. Most importantly, the Janus nanocomposites possess the unique dual independent mesopores with different pore sizes (2.1 nm and 3.5−5.5 nm) and hydrophobicity/hydrophilicity for loading of multiple guests. The distinct chemical properties of the silica sources and the different mesostructures of the dual-compartments are the necessary prerequisites for the formation of the Janus nanostructure. With the assistance of the near-infrared (NIR) to ultraviolet/visible (UV−vis) optical properties of UCNPs and heat-sensitive phase change materials, the dual-compartment Janus mesoporous silica nanocomposites can be further applied into nanobiomedicine for heat and NIR light bimodal-triggered dual-drugs controllable release. It realizes significantly higher efficiency for cancer cell killing (more than 50%) compared to that of the single-triggered drugs delivery system (∼25%).

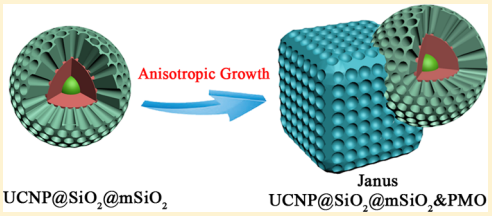

INTRODUCTION

Most recently, combined therapy with dual-drugs of different therapeutic effects shows excellent performance in the treatment of diseases, especially in drug-resistant cancer treatments.[1,2] To realize the best therapeutic effect, the species and doses of drugs should be optimized at different clinical manifestations and periods in the treatment. One of the main challenges of combined therapy is to control the release of each drug independently. However, simple drug delivery systems cannot fulfill the requirements of this combined therapy, because the widely used carriers, such as mesoporous silica (mSiO_2) nanoparticles,[3−7] hollow structured nanoparticles,[8−12] yolk−shell nanoparticles,[1,13−15] etc. normally possess symmetrical geometry with limited single storage space available for the loading of multiple drug species. When dual-drugs are simultaneously loaded in the single storage space, the release of each drug cannot be controlled independently. In addition, the loaded multidrugs may interact with each other leading to undesirable adverse effects, especially for drugs with different chemical properties (e. g., hydrophilicity/hydrophobicity, acidity/basicity, etc.).[16] Therefore, developing multicompartment carriers with independent storage spaces for the loading of multiple drugs is critically desired. The Janus nanostructure, possessing dual surface structures, is anisotropic in composition, shape, and surface chemistry, which is ideally suited for dual-guests attaching to different domains of the Janus particles. Furthermore, functionally distinct surfaces of Janus particles can also be used to selectively conjugate with specific triggers for individual release control of the dual-guests. However, the Janus nanocomposites obtained previously were mainly based on solid or dense polymers, SiO_2, etc. which could not provide enough storage space for guest molecules loading;[16−20] the synthesis of the dual-compartment Janus mesoporous composites especially with multifunctionality has never been reported yet.

In this work, the multifunctional dual-compartment Janus mesoporous silica nanocomposites of UCNP@SiO_2@mSiO_2&PMO (UCNP, upconversion nanoparticle = NaGdF_4:Yb,Tm@NaGdF_4, mSiO_2 = mesoporous silica shell, PMO = periodic mesoporous organosilica) have been successfully prepared for the first time by a novel anisotropic island nucleation and growth approach with the ordered mesostructure. The new anisotropic growth yields unique asymmetric Janus nanocomposites with a very uniform size of ∼300 nm, high surface area of ∼1290 m^2/g, and dual distinguished domains of hydrophilic composites (UCNP@SiO_2@mSiO_2) and the hydrophobic component (PMO) combined into one. The Janus nanocomposites not only possess an excellent NIR-to-UV−vis upconversion optical property from the UCNPs, but

Received: August 25, 2014
Published: September 24, 2014

   dx.doi.org/10.1021/ja508733r | J. Am. Chem. Soc. 2014, 136, 15086−15092

also provide UCNP@SiO_2@mSiO_2 nanospheres and PMO single-crystal nanocubes dual independent mesopores for dual guests loading. Advantaged by the unique Janus and dual-mesoporous structure, the dual-compartment Janus mesoporous silica nanocomposites can be further modified with azobenzene (Azo) (UV−vis light sensitive) and 1-tetradecanol (heat sensitive) molecules and applied to nanobiomedicine for heat and NIR light bimodal-triggered dual-drugs controllable release, and realize significantly excellent cancer cell killing efficiency (more than 50%), much higher than that of the single-triggered drugs delivery system (~25%).

EXPERIMENTAL SECTION

Synthesis of Core@Shell UCNP@SiO_2 Nanoparticles. First, 6.7 mL of otcanol and 12 mL of trixton X-100 were dispersed in 50 mL of cyclohexane by sonication and stirring. Then, 1.0 mL of (10 mg/mL) UCNPs cyclohexane solution was added into the above mixture. The resultant solution was stirred for 15 min, and then 0.4 mL of (28 wt %) ammonium hydroxide solution was added to form a reverse microemulsion solution. After stirring for 30 min, 0.3 mL of TEOS was added, and the resultant reaction was aged for 16 h under stirring. The final products (UCNP@SiO_2 nanoparticles) were collected by centrifuging and washed by water and ethanol several times. The core@shell UCNP@SiO_2 nanoparticles were finally dispersed in 30 mL of water for the further coating of mesoporous silica (mSiO_2) shells.

Synthesis of Core@Shell@Shell UCNP@SiO_2@mSiO_2 with Azo-modification. In brief, 30 mL of the core@shell UCNP@SiO_2 nanoparticles in solution prepared in the previous section (~50 mg) was added into the solution containing 48 mL of water, 48 mL of ethanol, 240 mg of CTAB, and 0.48 mL of ammonia aqueous solution (28 wt %). When the homodispersed solution was formed after stirring for 1 h, 0.4 mL of TEOS was added dropwise with continuous stirring and the reaction proceeded for 4 h to obtain the core@shell@shell UCNP@SiO_2@mSiO_2 nanoparticles. The products were collected by centrifugation, washed with ethanol and water, and dispersed in 20 mL of ethanol. The synthesis of the Azo-modified core@shell@shell UCNP@SiO_2@mSiO_2 nanoparticles was similar to the above procedure except that TEOS and Azo-coupled isocyanatopropylethoxysilane (Azo-ICPES, prepared according to the literature)[35,36] were used as the mixed silicon precursors instead of pure TEOS. The volume ratio between TEOS and Azo-ICPES was set at 19:1. It was calculated from UV−vis spectra that the Azo-modified UCNP@SiO_2@mSiO_2 nanoparticles contain about 3.9 wt % of the azobenzene derivatives.

Synthesis of Janus Nanocomposites UCNP@SiO_2@mSiO_2&PMO. The synthesis of the Janus nanocomposites UCNP@SiO_2@mSiO_2&PMO was based on the Stöber method.[37] Typically, 5.0 mL of the core@shell@shell UCNP@SiO_2@mSiO_2 nanoparticles (~90 mg) in solution obtained above was added into a solution containing 75 mL of water, 150 mg of CTAB and 1.8 mL of ammonia aqueous solution (28 wt %). The mixture was turned to a homodispersed solution after being stirred for 30 min. Then, 0.1 mL of BTEE was added dropwise with continuous stirring, and the reaction proceeded for 3 h. The final products, Janus mesoporous nanocomposites, UCNP@ SiO_2@mSiO_2&PMO, were collected by centrifugation, washed with ethanol and water, and dispersed in ethanol.

Post-treatment of the Janus Nanocomposites UCNP@SiO_2@mSiO_2&PMO. In our synthesis, the Janus mesoporous nanocomposites UCNP@SiO_2@mSiO_2&PMO obtained above underwent a post-ethanol-thermal treatment at 55 °C for about 4 h before the removal of CTAB surfactant templates. It could be noted that this post-treatment was necessary to increase the degree of cross-linking in the silica frameworks (Supporting Information, Figure S19). After the post-treatment, the mesostructural template of CTAB surfactant was extracted out of the mesopores by using NH_4NO_3 ethanol solution (2.0 g/L) for three times at a periodic 4 h each time.

Brief Guideline for the Fabrication of the Drug Delivery System. Owing to the presence of organic ethyl group in the PMO crystal pore frameworks, the Janus mesoporous nanocomposites possess distinct surface chemistry between the core@shell@shell UCNP@SiO_2@mSiO_2 and PMO crystal components, especially with regard to hydrophilicity/hydrophobicity. So, we selected hydrophobic paclitaxel and hydrophilic doxorubicin (DOX) as model drugs, which were commonly used in treatments of cancer cells. The hydrophilic DOX molecules were loaded first. Because of the relative hydrophilicity of the core@shell@shell UCNP@SiO_2@mSiO_2 components in the Janus nanocomposites, DOX molecules were preferentially adsorbed in the mesopore channels of the core@shell@shell UCNP@SiO_2@mSiO_2 parts and locked by the Azo switch. In addition, it was worthy to mention that the loading process of DOX molecules could be accelerated by the alternative radiation with UV and vis light due to the rotation-inversion movement of the Azo molecules. The residual DOX molecules in the mesoporous PMO crystal parts were easily washed off. Afterward, the hydrophobic paclitaxel molecules were introduced and absorbed in the mesopore frameworks of the mesoporous PMO crystal components. Finally, 1-tetradecanol PCM was used as another switch to control the release of the hydrophobic paclitaxel molecules.

RESULTS AND DISCUSSION

As shown in Figure 1, each Janus nanocomposite consists of four parts: (1) the NIR-to-UV−vis UCNP core, (2) concentric

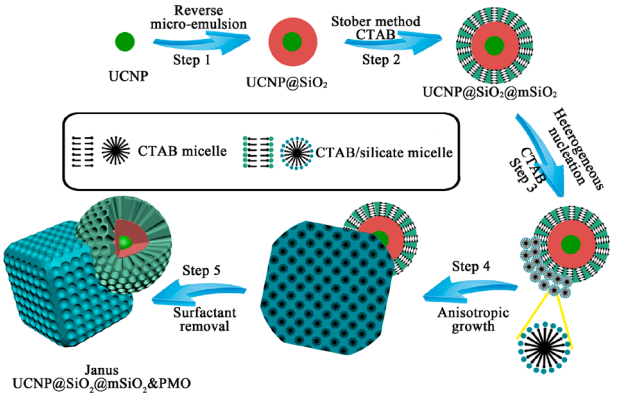

Figure 1. Synthetic procedure for the dual-compartment Janus mesoporous silica nanocomposites UCNP@SiO_2@ mSiO_2&PMO by the anisotropic island nucleation and growth method. UCNP = $NaGdF_4$:Yb,Tm@$NaGdF_4$, mSiO_2 = mesoporous silica shell, PMO = periodic mesoporous organosilica.

condense SiO_2 shells, and (3) ordered mesoporous silica (mSiO_2) shells with radial mesopore channels, (4) the single-crystal PMO nanocubes formed by the novel anisotropic growth approach of the ordered mesostructures on the surface of the core@shell@shell UCNP@SiO_2@mSiO_2 nanoparticles. The former three parts constitute a hydrophilic core@shell@shell structure with multifunctionality, the latter (part 4) possesses caged mesopores and hydrophobic organic functional group in the frameworks. Monodispersed UCNPs, β-$NaGdF_4$:25%Yb,0.5%Tm@$NaGdF_4$, with a uniform size of ~45 nm and morphology of hexagonal nanodisks were synthesized by using the successive layer-by-layer (SLBL) strategy and further used as the initial core (Supporting Information, Figure S1).[21] Because of the hydrophobic surface of the obtained UCNPs, a dense silica layer with a thickness of ~25 nm was coated on the UCNP nanodisks using a reverse microemulsion method to form the hydrophilic core@shell UCNP@SiO_2 nanoparticles (Step 1, Supporting Information,

dx.doi.org/10.1021/ja508733r | J. Am. Chem. Soc. 2014, 136, 15086−15092

Figure S2A).[13,22] Afterward, an ordered mesoporous $mSiO_2$ shell with a thickness of ~30 nm and concentric radial mesopore channels was uniformly coated around the core@shell UCNP@SiO_2 nanoparticles by using hexadecyltrimethylammonium bromide (CTAB) as a mesostructural template (Step 2, Supporting Information, Figure S2B). N_2 sorption isotherms of the core@shell@shell UCNP@SiO_2@$mSiO_2$ (Supporting Information, Figure S3) exhibit a type-IV curve with the H2/H4 hybrid hysteresis loop with a uniform mesopore size of ~2.4 nm, and the Brunauer–Emmett–Teller (BET) surface area is calculated to be ~800 m^2 g^{-1}. Finally, through the novel anisotropic island nucleation and growth approach by using the same cationic surfactant (CTAB) as a template and organic silane precursor (1,2-bis(triethoxysilyl)-ethane, BTEE) as a silica source (Step 3, 4), the single-crystal PMO nanoparticles with cubic morphology could be nucleated and grown on one side of the surface of the uniform UCNP@SiO_2@$mSiO_2$ particles, and further wrap up and attach on the part spherical core@shell@shell structured UCNP@SiO_2@$mSiO_2$ nanoparticles to realize the Janus nanocomposites UCNP@SiO_2@$mSiO_2$&PMO.

Transmission electron microscopy (TEM) images (Figure 2A–C, Supporting Information, Figure S4) of the obtained

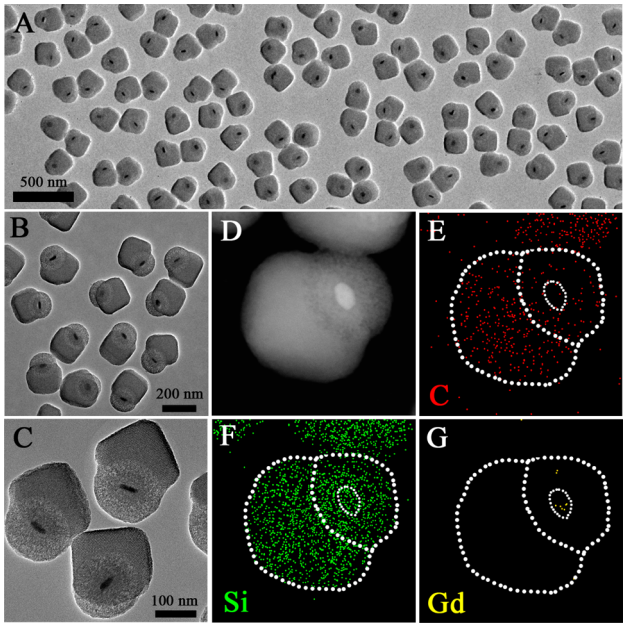

Figure 2. (A–C) TEM images with different magnifications of the obtained UCNP@SiO_2@$mSiO_2$&PMO Janus nanocomposites. (D–G) Dark field TEM images of one single UCNP@SiO_2@$mSiO_2$&PMO Janus nanoparticle (D) and energy-dispersive X-ray spectroscopy element mapping of C (E), Si (F), and Gd (G) elements in one UCNP@SiO_2@$mSiO_2$&PMO Janus nanoparticle.

nanoparticles show an obvious asymmetric Janus nanostructure with a very uniform size of ~300 nm. The Janus nanocomposites are composed by closely connected UCNP@SiO_2@$mSiO_2$ concentric core@shell@shell nanosphere (~150 nm in diameter) and a single-crystal PMO nanocube (~180 nm in edge length). As shown in Figure 2C, the Janus nanoparticles possess two distinct mesopore structures, the radial mesopore channels of the core@shell@shell UCNP@SiO_2@$mSiO_2$ nanospheres and highly ordered cubic mesopores of the single-crystal PMO nanocubes. Elemental mapping of one-single nanoparticle clearly shows the composition and Janus geometry (Figure 2D–G). All the expected elements, including carbon (C) (from the PMO and residual organic surfactant templates), silicon (Si) (from the PMO frameworks, SiO_2 and $mSiO_2$ shells), and gadolinium (Gd) (from the UCNP core) can be detected and matched well with the relative positions in the Janus nanocomposite. Because of the representative organic–inorganic hybrid mesostructure of the PMO single-crystals, the C distribution in the PMO nanocube domain is obviously higher than that in the core@shell@shell UCNP@SiO_2@$mSiO_2$ nanosphere domain (Figure 2E). Furthermore, it is found that the presence of the CTAB surfactants in the radial mesopore channels of the core@shell@shell UCNP@SiO_2@$mSiO_2$ particles before the growing of PMO components is very important for the formation of the Janus nanostructure due to the etching effect during the hydrolysis of the organic silane precursors. If the CTAB surfactant template in the radial mesopore channels of the core@shell@shell UCNP@SiO_2@$mSiO_2$ nanoparticles was extracted out before it was used for the anisotropic growth of PMO crystals, the mesoporous silica $mSiO_2$ layers could be totally etched during PMO nucleation and deposition (Supporting Information, Figure S5). Our results confirm that an etching effect indeed exists during the hydrolysis of the organic silane precursors, and this etching effect can be relieved under the protection of CTAB surfactant templates inside the mesopore channels.

According to statistic results of the relative positions between the two domains of Janus nanoparticles, we considered that the single-crystal PMO nanocubes randomly attach and wrap on the surface of the UCNP@SiO_2@$mSiO_2$ core@shell@shell nanospheres (Figure 3A,B, Supporting Information, Figure S6), meaning that there is no lattice-match relationship between the radial mesopore channels and the caged mesopores of the PMO single-crystal nanocubes. In other words, PMO crystals can nucleate randomly on the surface of the core–shell nanospheres, anisotropically grow along one-direction, and finally wrap up randomly. To certify this assumption, the core@shell UCNP@SiO_2 nanoparticles without the radial mesopore silica shells were used as the initial seed instead of the core@shell@shell UCNP@SiO_2@$mSiO_2$ nanoparticles. It shows that similar Janus nanoparticles can also be obtained (Supporting Information, Figure S7), indicating that the attachment of the single-crystal PMO nanocube on the surface of the nanosphere is a random process and irrelevant to lattice-match between the mesopore channels of the two domains.[23] The small-angle X-ray scattering (SAXS) patterns show three well-resolved scattering peaks at q-values of 1.35, 1.51, and 1.65 nm^{-1}, corresponding to the 200, 210, and 211 reflections of the cubic mesostructure ($Pm\bar{3}n$) with a unit cell parameter of 9.31 nm (Figure 3C). TEM images along with the corresponding fast Fourier transform (FFT, Figure 3D–F) of the resultant Janus mesoporous nanocomposites show that the PMO domains possess highly ordered mesopores with a single-crystal structure. The FFT patterns of the single-crystals along the [001], [111] and [210] zone axes show that the mesostructure of the PMO parts is a simple cubic structure with a space group $Pm\bar{3}n$, which is consistent with the results from the SAXS patterns (Figure 3C).

N_2 sorption isotherms of the obtained Janus nanocomposites exhibit typical type-IV curves with a rapid increase in the adsorption branch at a relative pressure of 0.2–0.4, clearly indicating uniform mesopores (Supporting Information, Figure S8A). The BET surface area is estimated to be ~1290 m^2/g,

dx.doi.org/10.1021/ja508733r | J. Am. Chem. Soc. 2014, 136, 15086–15092

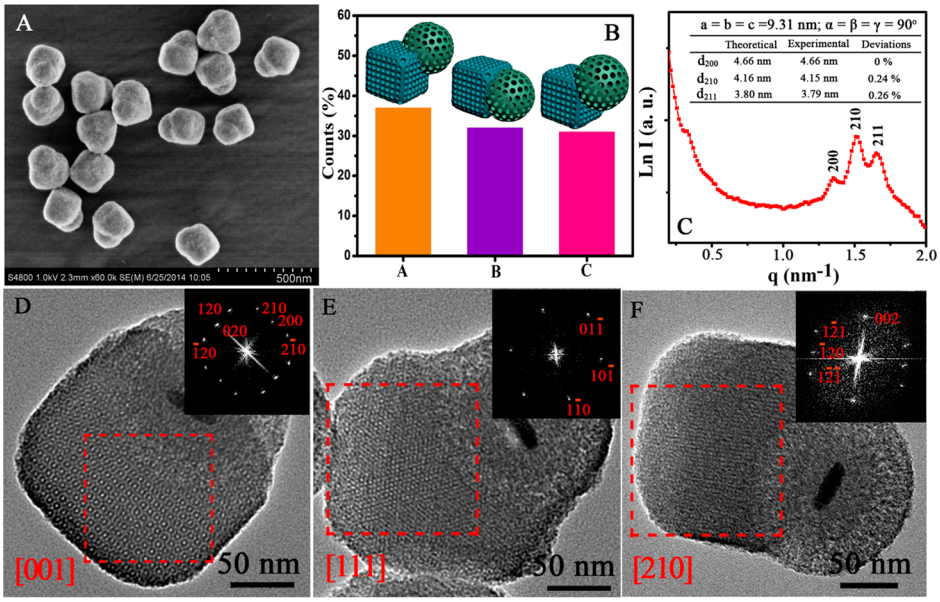

Figure 3. (A) SEM images of the obtained UCNP@SiO_2@mSiO_2&PMO Janus nanocomposites. (B) The statistic results of the relative positions between the core@shell@shell UCNP@SiO_2@mSiO_2 nanosphere domain and PMO single-crystal nanocube domain of Janus nanoparticles: the nanosphere attached on the vertex, edge, or face of the nanocube. (C) The SAXS pattern of the Janus mesoporous nanocomposites (inset: the theoretical and experimental *d*-spacing values of different planes obtained from the cell parameter and SAXS pattern). (D–F) The TEM images along with the corresponding fast Fourier transform of the Janus nanocomposite along [001] (D), [111] (E), and [210] (F) zone axis.

which is between the values of the bare core@shell@shell UCNP@SiO_2@mSiO_2 particles (800 m^2/g) (Supporting Information, Figure S3) and the PMO single-crystal nanocubes (1520 m^2/g) (Supporting Information, Figure S9). This means that the mass ratio between the UCNP@SiO_2@mSiO_2 domain and PMO single-crystal nanocube domain in a single Janus nanoparticle is about 1:2. From the pore size distribution curve (Supporting Information, Figure S8B) obtained by the Barrett–Joyner–Halenda (BJH) method, the mesoporous Janus nanocomposites exhibit a rather narrow mesopore size distribution with an average diameter of ~2.1 nm and a broad size distribution in the range of 3.5–5.5 nm, which are derived from the ordered mesopores of the PMO single-crystal domains and radial mesopore channels of the core@shell@shell UCNP@SiO_2@mSiO_2 domains, respectively. The pore size distribution of the parent UCNP@SiO_2@mSiO_2 core@shell@shell nanoparticles (~2.4 nm) before the growth of the PMO crystals is much narrower and smaller than that of the Janus nanocomposites (3.5–5.5 nm) (Supporting Information, Figure S8B, S10). We consider that this result is from the etching effect during the hydrolysis of the organic silicon precursors, which has been demonstrated above.

As far as we know, it is difficult to fine-tune surface tension and lattice mismatch between silica and the core materials to form the Janus nanostructures because of the amorphous nature of silica with isotropic properties. Mesoporous silica materials have attracted a great deal of attention because of their versatility in surface tension and pore lattice parameters. To realize the formation of mesoporous-silica-based Janus nanoparticles, the solution grown synthesis route for the fabrication of inorganic nanocrystals-based heterodimer Janus nanostructures (such as Au–Fe_3O_4,[24] CdS-FePt,[25] PbSe-Au,[26] etc.)[27,28] provides a clue that the distinct chemical composition and crystal structure are the necessary prerequisites for the formation of the Janus nanostructure. In our synthesis, two different silanes were used as the precursors for the formation of the different domains of the heterodimer Janus nanocomposites. One is tetraethyl orthosilicate (TEOS) for the synthesis of core@shell@shell UCNP@SiO_2@mSiO_2 domains, the other is organic silane [bis(triethoxysilyl)ethane, BTEE] for the following formation of the PMO crystal domains. Because of the distinct chemical structure between the two silanes, the BTEE lean toward anisotropic polymerization on the surface of the core@shell@shell UCNP@SiO_2@mSiO_2 domain. Furthermore, we also set the synthesis condition for the formation of a single crystal cubic mesophase domain with the presence of the structure-directing agent, which is distinguished from the radial mesochannels of the core@shell@shell UCNP@SiO_2@mSiO_2 domains. In such a case, rather than epitaxy from atomic structures, the mesostructures can be oriented by surfactants micelles and further induce the anisotropic epitaxial growth of the ordered PMO crystals. Through a surfactant-templating approach with the same cationic surfactant CTAB as a structure-directing agent, mesostructured CTAB/silicate micelles can be assembled and nucleated on the surfaces of the core@shell@shell structured UCNP@SiO_2@mSiO_2 nanospheres through a heterogeneous nucleation process. After the nucleation sites are formed, the growth manner of PMO crystals results in the different morphology of the nanocomposites, which is determined by the hydrolysis environment (especially the solvent) of BTEE and the mesostructures of the obtained PMO. After the CTAB/silicate micelles nucleated on the surfaces of the UCNP@SiO_2@mSiO_2 (in a small area, the surface of the nanospheres can be approximated as plane surface), the change in the total surface energy, $\Delta\sigma$, that accompanies the overall deposition process can be represented as

$$\Delta\sigma = \sigma_{\text{PMO-solvent}} + \sigma_{\text{PMO-SiO}_2} - \sigma_{\text{SiO}_2\text{-solvent}}$$

where $\sigma_{\text{PMO-solvent}}$ and $\sigma_{\text{SiO}_2\text{-solvent}}$ are the surface energies of the PMO and UCNP@SiO_2@mSiO_2 in solvent, and $\sigma_{\text{PMO-SiO}_2}$ is

dx.doi.org/10.1021/ja508733r | J. Am. Chem. Soc. 2014, 136, 15086–15092

the solid−solid interfacial energy between PMO and UCNP@SiO_2@mSiO_2 (Figure 4). Because of the representative

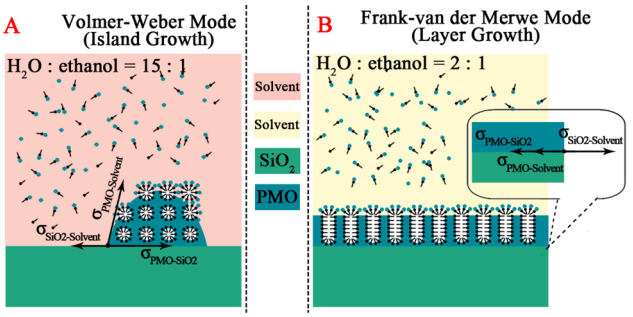

Figure 4. (A) The island growth of the cubic $Pm\bar{3}n$ mesostructured PMO on the core@shell@shell structured UCNP@SiO_2@mSiO_2 nanospheres in the H_2O/ethanol solvent (H_2O/ethanol = 15:1). (B) The layer growth of the radial mesoporous PMO on the core@shell@shell structured UCNP@SiO_2@mSiO_2 nanospheres in the H_2O/ethanol solvent (H_2O/ethanol = 2:1).

organic−inorganic hybrid structure of PMO, the surface energy of PMO ($\sigma_{PMO\text{-}solvent}$) in the H_2O/ethanol solvent increases as the volume percentage of H_2O increases. In contrast, the surface energy of the UCNP@SiO_2@mSiO_2 ($\sigma_{SiO2\text{-}solvent}$) decreases as the volume percentage of H_2O increases. As shown in Figure 4A, when the volume ratio of H_2O/ethanol reaches 15:1, $\sigma_{PMO\text{-}solvent}$ is larger than $\sigma_{SiO_2\text{-}solvent}$, causing $\Delta\sigma > 0$ ($\sigma_{PMO\text{-}SiO_2}$ is very low, because of the similar −Si−O−Si− components between PMO and UCNP@SiO_2@mSiO_2). It means that it is very difficult for the the CTAB/silicate micelles to spread on the surface of UCNP@SiO_2@mSiO_2. So, the energy barrier of the growth of PMO in the heterogeneous direction (i.e., UCNP@SiO_2@mSiO_2 direction) is much higher than that in the homogeneous directions (opposite to UCNP@SiO_2@mSiO_2 direction), which induces the anisotropic growth of the initial PMO nucleus. Through this anisotropic growth, the single-crystal PMO nanoparticles with uniform cube morphology can be formed and attached on the spherical UCNP@SiO_2@mSiO_2 seeds to realize the UCNP@SiO_2@mSiO_2&PMO Janus nanocomposites. This result is consistent with the classical island growth mode of Volmer−Weber[29,30] To further certify this anisotropic island growth mechanism of the PMO single-crystals, the volume ratio between H_2O and ethanol was decreased to 2:1, which caused the decrease of $\sigma_{PMO\text{-}solvent}$, increase of $\sigma_{SiO_2\text{-}solvent}$, and $\Delta\sigma < 0$. As a result, the spreading of PMO on the UCNP@SiO_2@mSiO_2 was much easier, resulting in a layer growth (Frank van der Merwe mode)[31] of PMO on the spherical UCNP@SiO_2@mSiO_2 and the formation of the concentric core@shell@shell@shell structured UCNP@SiO_2@mSiO_2@PMO nanocomposites (Figures 4B, 5A,B). It was found that the volume ratio between H_2O and ethanol could also influence the shape of the CTAB/silicate micelles. Compared with the cubic $Pm\bar{3}n$ mesostructure of the single-crystal PMO domains of the Janus nanocomposites, the concentric UCNP@SiO_2@mSiO_2@PMO nanoparticles show radial mesopore channels (Figure 5C). After etching condense silica shell and mesoporous silica shell of core@shell@shell@shell UCNP@SiO_2@mSiO_2@PMO and UCNP@SiO_2@ mSiO_2&PMO Janus nanoparticles by a post-hydrothermal treatment at 60 °C, the rattle-type UCNP@PMO nanoparticles (Figure 5D) and the nanocubes with ball-shaped

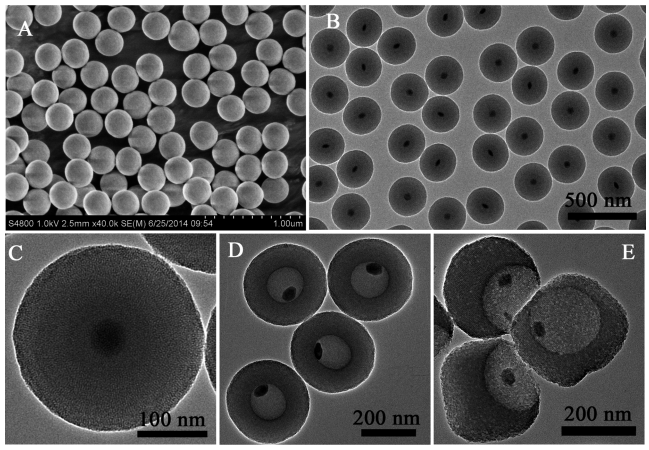

Figure 5. (A) SEM image of the obtained concentric core@shell@shell@shell UCNP@SiO_2@mSiO_2@PMO nanoparticles. (B, C) TEM images with different magnifications for the obtained concentric core@shell@shell@shell UCNP@SiO_2@mSiO_2@PMO nanoparticles. (D) TEM image of the rattle-type UCNP@PMO nanoparticles obtained after the etching condense silica shell and mesoporous silica shell by post-hydrothermal treatment of the core@shell@shell@shell UCNP@SiO_2@mSiO_2@PMO nanoparticles at 60 °C. (E) The nanocubes with ball-shaped depression obtained after the etching condense silica shell and mesoporous silica shell by post-hydrothermal treatment of the obtained Janus UCNP@SiO_2@mSiO_2&PMO nanoparticles at 60 °C.

depression (Figure 5E, Supporting Information, Figure S11) can be obtained, respectively. It further indicates the concentric structure of the core@shell@shell@shell UCNP@SiO_2@mSiO_2@PMO and the heterodimer Janus nanostructure of the UCNP@SiO_2@mSiO_2 &PMO nanocomposites.

As a proof of concept, the dual-compartment Janus mesoporous silica nanocomposites were further applied to nanobiomedicine for heat and upconversion luminescence triggered dual-drugs controllable release. First, the Janus nanocomposites were selectively modified with light sensitive Azo molecules in the radial mesopore channels of the core@shell@shell UCNP@SiO_2@mSiO_2 domains and heat sensitive phase change materials (PCM) 1-tetradecanol on the outer surface of the entire Janus nanoparticles (Figure 6A, Supporting Information, Figures S12−S16).[11,32−34] At below its melting point, the PCM 1-tetradecanol is in a solid state to completely block the passing of encapsulated species. When the temperature is raised beyond its melting point (38−39 °C), the PCM can be quickly melted to release the encapsulated species (Guest 1) in the hydrophobic PMO crystal domains. For the NIR-to-UV−vis upconversion luminescence sensitive Azo molecules, it can transform into the *cis*-isomer from the *trans* isomer under UV irradiation (~360 nm) and in contrast the *cis*-isomer can transform into the *trans*-isomer under irradiation of visible light (~450 nm). Upon absorption of NIR light (980 nm), the β-$NaGdF_4$:25%Yb,0.5%Tm@$NaGdF_4$ UCNP cores in core@shell@shell UCNP@SiO_2@mSiO_2 domains can emit photons in the UV−vis region (Supporting Information, Figure S17), which can be absorbed immediately by the photo-responsive Azo molecules in the mesopore frameworks of the core@shell@shell UCNP@SiO_2@mSiO_2 domains (Supporting Information, Figure S18). The reversible photoisomerization by simultaneous UV and visible light emitted by the UCNPs create continuous rotation-inversion movement. The back and forth wagging motion of the Azo molecules acts as a molecular impeller that propels the release of the encapsulated species

dx.doi.org/10.1021/ja508733r | J. Am. Chem. Soc. 2014, 136, 15086−15092

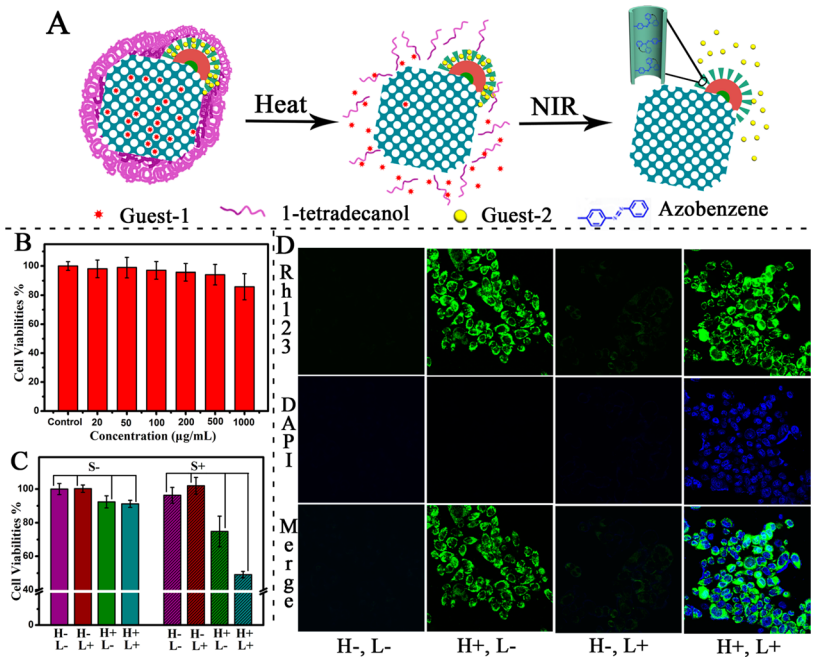

Figure 6. (A) Schematic presentation for dual-control drug release systems by using the dual-compartment mesoporous Janus nanocomposites. (B) MTT cell viability assay of Janus UCNP@SiO_2@mSiO_2&PMO nanocomposites on HeLa cells. (C) Cell viabilities of paclitaxel and DOX coloaded UCNP@SiO_2@mSiO_2-Azo&PMO−PCM Janus nanocomposites under the heat (H) and NIR light (L) treatment (S means sample). (D) Confocal laser scanning microscopy (CLSM) observations of the HeLa cells after incubation with the Rh123 (green) and DAPI (blue) coloaded mesoporous Janus nanocomposites with or without heat (H) and NIR light (L) stimuli.

(Guest 2) in the core@shell@shell structured UCNP@SiO_2@mSiO_2 mesopore channels.[32,33] The viability of HeLa cells after exposure to the UCNP@SiO_2@mSiO_2&PMO Janus nanocomposites at different concentrations was evaluated by cell-counting kit-8 (CCK-8) assay (Figure 6B). It can be seen that the viability of the cells is maintained at more than 90% even when the nanocomposite concentration increases to 500 μg/mL, indicating the high biocompatibility of the UCNP@SiO_2@mSiO_2&PMO Janus nanocomposites.

PMOs are the most representative hybrid porous materials with the organic/inorganic components completely and homogeneously distributed over the whole frameworks at the molecular level. Owing to presence of the ethyl group in the PMO pore frameworks, the Janus mesoporous nanocomposites possess two distinct surfaces chemistries between the core@shell@shell UCNP@SiO_2@mSiO_2 domains and PMO single-crystal domains, especially with regard to hydrophilicity/hydrophobicity. Therefore, hydrophobic paclitaxel and hydrophilic doxorubicin (DOX) were selected as model drugs and loaded in the mesopore channels of the PMO crystal domains and core@shell@shell structured UCNP@SiO_2@mSiO_2-Azo domains (see the Experiment Section for detail), respectively. 1-Tetradecanol PCM and Azo molecules were used as switches to control the release of the drugs. Then, the delicately designed dual-drugs controlled release studies were carried out by incubating the nanocomposites with HeLa cells to validate the feasibility of this drug delivery system *in vitro* (Figure 6C). The results show that the treatments with UCNP@SiO_2@mSiO_2-Azo&PMO−PCM Janus nanocomposites loaded with and without drugs do not make a significant decrease in the cell viability in the absence of stimuli of the switches, indicating the negligible releasing of the drug molecules. In contrast, the dual-drugs loaded UCNP@SiO_2@mSiO_2-Azo&PMO−PCM Janus nanocomposites upon heat treatment (~39 °C) show significantly enhanced cytotoxicity to the cancer cells (~25% killing efficacy), which can be ascribed to the opening of the first switch and the releasing of the paclitaxel molecules in the mesopores of the PMO crystal domains. Furthermore, if the heat and NIR light are introduced at the same time, both of the switches can be trigged to open. The paclitaxel and DOX molecules can be released at the same time, which induces the further increased cytotoxicity to the cancer cells (over 50% killing efficacy).

To further detect the heat and NIR responsive behavior of the two switches, Rhodamine 123 (Rh 123) (mitochondria staining reagent) and 4,6-diamino-2-phenyl indole (DAPI) (nucleus staining reagent) were chosen as the fluorescent probes and loaded into the PMO single-crystal domains and the core@shell@shell UCNP@SiO_2@mSiO_2 domains of the Janus nanocomposites, respectively (Figure 6D). In the absence of both heat and NIR light stimuli, the two dyes were locked in the mesopores of the Janus nanocomposites and no free dye molecules could be detected in the cell. Under identical experimental conditions but incubating the cell under the heat condition (~39 °C), Rh 123 molecules loaded in the caged mesoporous of the PMO crystal domains were detected in the cytoplasm, and no signal from DAPI molecules could be detected in the nucleus of the cells. In stark contrast, when the heat treatment and NIR light were introduced at the same time, bright green and blue photoluminescence from Rh 123 and DAPI molecules could be easily observed in the cytoplasm and nucleus of the cells. So, we can conclude that the release behavior of the dual-guest molecules loaded in different domains of the Janus mesoporous nanocomposites can be well controlled by the delicate designed drug delivery system. It is worth noting that small amounts of Rh 123 and DAPI molecules can leak from the Janus nanocomposites under the bare NIR light stimulation, which can be attributed to an

dx.doi.org/10.1021/ja508733r | J. Am. Chem. Soc. 2014, 136, 15086−15092

increase in temperature of the medium under the NIR irradiation.

CONCLUSIONS

In summary, multifunctional dual-compartment Janus mesoporous silica nanocomposites (UCNP@SiO_2@mSiO_2&PMO) have been for the first time synthesized on the basis of the novel anisotropic island nucleation and growth of ordered silica mesostructures. The asymmetric Janus nanocomposites are composed by upconversion nanoparticles functionalized core@shell@shell structured UCNP@SiO_2@mSiO_2 nanoparticles and PMO single-crystal nanocubes and show very uniform sizes of ~300 nm and high surface areas of ~1290 m^2/g. Most importantly, the Janus nanocomposites possess the unique dual independent mesopores with bimodal pore sizes (2.1 and 3.5−5.5 nm) and hydrophobicity/hydrophilicity domains for loading of dual guests. With the assistance of the unique NIR-to-UV−vis optical properties of the UCNP cores and heat-sensitive properties of PCM molecules, the Janus mesoporous silica nanocomposites can be further applied into nanobiomedicine for heat and NIR light bimodal triggered dual-drugs release, and the cancer cell killing efficiency (more than 50%) is significantly higher than that for the single triggered drugs delivery system (~25%). We believe that our discovery of the Janus mesoporous silica nanocomposites could lead to further development of new concepts and architectures of nanocarriers, thus allowing more opportunities in multidrug delivery and combined therapy.

ASSOCIATED CONTENT

Supporting Information

Supplementary experimental section and data. This material is available free of charge via the Internet at http://pubs.acs.org.

AUTHOR INFORMATION

Corresponding Authors

dyzhao@fudan.edu.cn

zhang_fan@fudan.edu.cn

Notes

The authors declare no competing financial interest.

ACKNOWLEDGMENTS

The work was supported by NSFC (Grant No. 21322508, 21101029, 21273041, 21210004), China National Key Basic Research Program (973 Project) (No. 2013CB934100, 2012CB224805, 2010CB933901), the Shanghai Rising-Star Program (12QA1400400), Program for New Century Excellent Talents in University (NCET),and the State Key Laboratory of Pollution Control and Resource Reuse Foundation (No. PCRRF12001). This work was also supported by NSTIP strategic technologies programs (Project No. 12-NAN2544-02) in the Kingdom of Saudi Arabia.

REFERENCES

(1) Fang, Y.; Zheng, G.; Yang, J.; Tang, H.; Zhang, Y.; Kong, B.; Lv, Y.; Xu, C.; Asiri, A. M.; Zi, J.; Zhang, F.; Zhao, D. Y. *Angew. Chem., Int. Ed.* **2014**, *126*, 5470−5474.

(2) He, Q. J.; Gao, Y.; Zhang, L. X.; Zhang, Z. W.; Gao, F.; Ji, X. F.; Li, Y. P.; Shi, J. L. *Biomaterials* **2011**, *32*, 7711−7720.

(3) Xing, L.; Zheng, H.; Cao, Y.; Che, S. *Adv. Mater.* **2012**, *24*, 6433−6437.

(4) Qian, R.; Ding, L.; Ju, H. *J. Am. Chem. Soc.* **2013**, *135*, 13282−13285.

(5) Zhang, J.; Yuan, Z. F.; Wang, Y.; Chen, W. H.; Luo, G. F.; Cheng, S. X.; Zhuo, R. X.; Zhang, X. Z. *J. Am. Chem. Soc.* **2013**, *135*, 5068−5073.

(6) He, Q.; Shi, J. *Adv. Mater.* **2014**, *26*, 391−411.

(7) Kang, X.; Cheng, Z.; Li, C.; Yang, D.; Shang, M.; Ma, P.; Li, G.; Liu, N.; Lin, J. *J. Phys. Chem. C* **2011**, *115*, 15801−15811.

(8) Zhao, Y.; Lin, L. N.; Lu, Y.; Chen, S. F.; Dong, L.; Yu, S. H. *Adv. Mater.* **2010**, *22*, 5255−5259.

(9) Chen, Y.; Chen, H.; Zeng, D.; Tian, Y.; Chen, F.; Feng, J.; Shi, J. *ACS Nano* **2010**, *4*, 6001−6013.

(10) Fu, J.; Chen, T.; Wang, M.; Yang, N.; Li, S.; Wang, Y.; Liu, X. *ACS Nano* **2013**, *7*, 11397−11408.

(11) Hyun, D. C.; Lu, P.; Choi, S. I.; Jeong, U.; Xia, Y. *Angew. Chem., Int. Ed.* **2013**, *52*, 10468−10471.

(12) Chen, Y.; Xu, P. F.; Chen, H. R.; Li, Y. S.; Bu, W. B.; Shu, Z.; Li, Y. P.; Zhang, J. M.; Zhang, L. X.; Pan, L. M.; Cui, X. Z.; Hua, Z. L.; Wang, J.; Zhang, L. L.; Shi, J. L. *Adv. Mater.* **2013**, *25*, 3100−3105.

(13) Zhang, F.; Braun, G. B.; Pallaoro, A.; Zhang, Y.; Shi, Y.; Cui, D.; Moskovits, M.; Zhao, D. Y.; Stucky, G. D. *Nano Lett.* **2012**, *12*, 61−67.

(14) Fan, W.; Shen, B.; Bu, W.; Chen, F.; Zhao, K.; Zhang, S.; Zhou, L.; Peng, W.; Xiao, Q.; Xing, H.; Liu, J.; Ni, D.; He, Q.; Shi, J. *J. Am. Chem. Soc.* **2013**, *135*, 6494−6503.

(15) Liu, J.; Bu, J.; Bu, W.; Zhang, S.; Pan, L.; Fan, W.; Chen, F.; Zhou, L.; Peng, W.; Zhao, K.; Du, J.; Shi, J. *Angew. Chem., Int. Ed.* **2014**, *53*, 4551−4555.

(16) Wang, F.; Pauletti, G. M.; Wang, J.; Zhang, J.; Ewing, R. C.; Wang, Y.; Shi, D. *Adv. Mater.* **2013**, *25*, 3485−3489.

(17) Chen, T.; Chen, G.; Xing, S.; Wu, T.; Chen, H. *Chem. Mater.* **2010**, *22*, 3826−3828.

(18) Ohnuma, A.; Cho, E. C.; Camargo, P. H.; Au, L.; Ohtani, B.; Xia, Y. *J. Am. Chem. Soc.* **2009**, *131*, 1352−1353.

(19) Chen, T.; Yang, M.; Wang, X.; Tan, L. H.; Chen, H. *J. Am. Chem. Soc.* **2008**, *130*, 11858−11859.

(20) Díez, P.; Sánchez, A.; Gamella, M.; Martínez-Ruíz, P.; Aznar, E.; Torre, C.; Murguía, J. R.; Martínez-Máñez, R.; Villalonga, R.; Pingarrón, J. M. *J. Am. Chem. Soc.* **2014**, *136*, 9116−9123.

(21) Li, X.; Shen, D.; Yang, J.; Yao, C.; Che, R.; Zhang, F.; Zhao, D. *Chem. Mater.* **2013**, *25*, 106−112.

(22) Garcia, J. V.; Yang, J.; Shen, D.; Yao, C.; Li, X.; Wang, R.; Stucky, G. D.; Zhao, D.; Ford, P. C.; Zhang, F. *Small* **2012**, *8*, 3800−3805.

(23) Suteewong, T.; Sai, H.; Hovden, R.; Muller, D.; Bradbury, M. S.; Gruner, S. M.; Wiesner, U. *Science* **2013**, *340*, 337−341.

(24) Yu, H.; Chen, M.; Rice, P. M.; Wang, S. X.; White, R.; Sun, S. *Nano Lett.* **2005**, *5*, 379−382.

(25) Gu, H.; Zheng, R.; Zhang, X.; Xu, B. *J. Am. Chem. Soc.* **2004**, *126*, 5664−5665.

(26) Yang, J.; Elim, H. I.; Zhang, Q.; Lee, J. Y.; Ji, W. *J. Am. Chem. Soc.* **2006**, *128*, 11921−11926.

(27) Costi, R.; Saunders, A. E.; Banin, U. *Angew. Chem., Int. Ed.* **2010**, *49*, 4878−4897.

(28) Wang, C.; Xu, C.; Zeng, H.; Sun, S. *Adv. Mater.* **2009**, *21*, 3045−3052.

(29) Peng, Z.; Yang, H. *Nano Today* **2009**, *4*, 143−164.

(30) Goebl, J. A.; Black, R. W.; Puthussery, J.; Giblin, J.; Kosel, T. H.; Kuno, M. *J. Am. Chem. Soc.* **2008**, *130*, 14822−14833.

(31) Carbone, L.; Cozzoli, P. D. *Nano Today* **2010**, *5*, 449−493.

(32) Liu, J.; Bu, W.; Pan, L.; Shi, J. *Angew. Chem., Int. Ed.* **2013**, *52*, 4375−4379.

(33) Angelos, S.; Choi, E.; Vögtle, F.; Cola, L. D.; Zink, J. I. *J. Phys. Chem. C* **2007**, *111*, 6589−6592.

(34) Aznar, E.; Mondragón, L.; Ros-Lis, J. V.; Sancenón, F.; Marcos, M. D.; Martínez-Máñez, R.; Soto, J.; Pérez-Payá, E.; Amorós, P. *Angew. Chem., Int. Ed.* **2011**, *50*, 11172−11175.

(35) Lu, J.; Choi, E.; Tamanoi, F.; Zink, J. I. *Small* **2008**, *4*, 421−426.

(36) Zhu, Y.; Fujiwara, M. *Angew. Chem., Int. Ed.* **2007**, *46*, 2241−2244.

(37) Stöber, W.; Fink, A.; Bohn, E. *J. Colloid Interface Sci.* **1968**, *26*, 62−69.